Reviewer 1:

This study uses extreme swell warnings issued by the Peruvian Navy and ERA5 reanalysis data to analyze the atmospheric circulation precursors of extreme swell events in the Southern Hemisphere (5 events) and Northern Hemisphere (6 events). It reveals the hemispherically differentiated configuration of the polar-front jet and the subtropical jet, and employs a flow-analogue approach to assess the impact of climate change on event intensity. The research topic has clear practical value, the methodology is relatively advanced, and the results are directly relevant to swell early warning along the Peruvian coast. The overall scientific quality is good; however, there are several methodological limitations and deficiencies in result interpretation. It is recommended that the manuscript be revised before acceptance.

Thank you for your thoughtful and constructive review. We greatly appreciate your positive assessment of the study's practical relevance, methodological approach, and its contribution to improving swell early warning along the Peruvian coast. We also value your insightful comments regarding the methodological limitations and the interpretation of results. These observations are very helpful, and we will carefully address them in a revised version of the manuscript.

1. Only five SH events and six NH events are included, spanning 17 years. The conclusions may be affected by interdecadal bias, raising doubts about their generalizability. It is recommended to extend the event selection period back to beyond 1980 (using earlier wave reanalysis or historical documentary records) to increase the number of events.

We agree that the limited number of events may reduce the generalizability of the results and that interdecadal variability may affect the composite patterns, particularly in the Northern Hemisphere.

However, the event catalogue used in this study is intentionally restricted to the homogeneous operational archive currently available from DIHIDRONAV, which provides consistently classified anomalous-swell warnings for the 2008–2025 period. Extending the sample back to earlier decades would require a retrospective reconstruction of historical events using non-uniform documentation and without a directly comparable classification scheme, which could introduce substantial inhomogeneity and misclassification bias.

We also examined whether historical swell events reported for the Chilean coast could be incorporated into the analysis. However, those records are not classified under the same wave-based operational criteria used by DIHIDRONAV for the Peruvian coast, but rather under a different intensity framework more closely linked to reported impacts and damages. Since the present study is specifically focused on extreme swell events affecting Peru, mixing both catalogues would reduce the internal consistency of the event definition.

Following the referee's suggestion, in the revised manuscript we will explicitly acknowledge this limitation and temper the scope of the conclusions. In particular, we will clarify that the identified patterns should be interpreted as characteristic of a homogeneous benchmark sample of Peruvian extreme-swell events, rather than as a complete climatology of all historical extreme swells in the southeast Pacific. We will also include a sentence in the Conclusion noting that future work should aim

to reconstruct and consistently reclassify pre-2008 historical events in order to assess the robustness of these results under longer-term interdecadal variability **(L569-572)**.

2. The study uses a fixed great-circle distance and a constant wave period (16–20 s), without considering nonlinear dissipation, refraction, diffraction, or background currents (e.g., equatorial currents) during wave propagation. The 8- to 11-day composite window for NH events may incorporate substantial unrelated meteorological noise. It is recommended to use at least one wave hindcast model (e.g., WAVEWATCH III) to simulate one or two representative events (one from each hemisphere), validating the wave height, period, and travel time from the generation region to the Peruvian coast. If such modelling is not feasible, a sensitivity analysis should be added: recompute the travel-time window using different wave periods (14–22 s) and great-circle distances (±10%), and assess the sensitivity of the composite fields to window shifts.

We agree that the manuscript does not describe with sufficient detail how the representative source-to-coast distances were obtained.

In the revised manuscript, we will clarify that the representative fetch locations were identified event by event from ERA5 sequences of sea-level pressure and 10-m wind fields during the days preceding the onset of the DIHIDRONAV swell warnings **(L87-97)**. For each event, we inspected the preconditioning period indicated by operational knowledge of swell propagation toward Peru and identified the region where the pressure gradient was strongest and where the most intense and persistent surface-wind vectors were oriented toward the Peruvian coast. The central coordinates of these fetch regions were then recorded for each event, and their arithmetic mean was used to define a representative source point for the SH and NH composites.

The source-to-coast distance was then calculated as the great-circle distance between this representative fetch point and a coastal reference point off Peru, and the corresponding travel times were estimated using deep-water group-velocity theory with representative swell periods taken from the empirical range commonly reported for long-period anomalous swells affecting Peru.

We agree with the referee that this is a simplified approach and does not explicitly account for nonlinear dissipation, refraction, diffraction, or background currents during propagation. For this reason, and following the referee's suggestion, in the revised manuscript we will include a sensitivity analysis in which the travel-time windows will be recomputed using a wider range of swell periods and a ±10% perturbation of the representative great-circle distance **(Figs. S2-S5, S13-S16)**. We will then compare the resulting composites in order to assess the robustness of the large-scale atmospheric patterns to the assumed propagation window **(L193-195, L334-337)**.

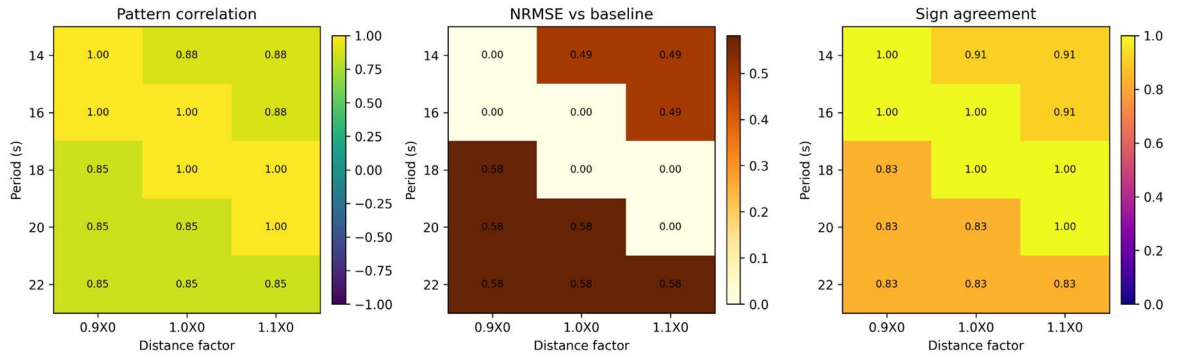

Figure S3. *Summary sensitivity metrics for the Southern Hemisphere SLP composites relative to the baseline window.* Heat maps show pattern correlation, normalized root-mean-square error, and sign agreement for each combination of assumed swell period and distance factor.

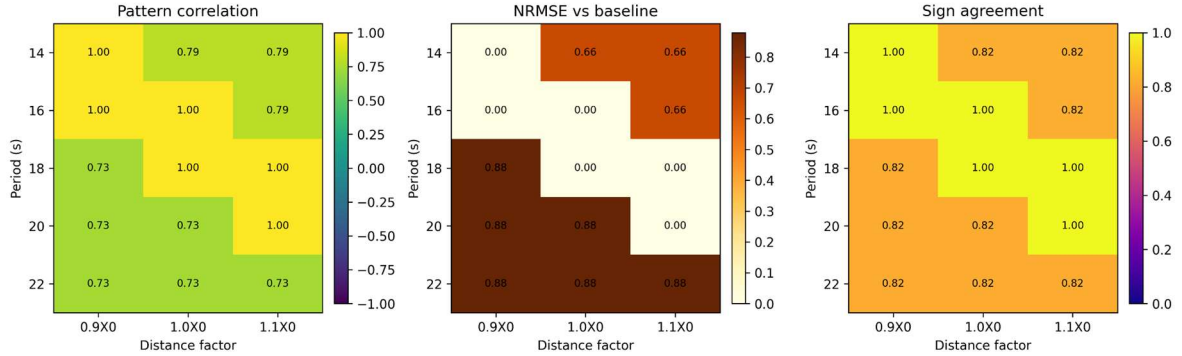

Figure S5. *Summary sensitivity metrics for the Southern Hemisphere SHWW composites relative to the baseline window.* Heat maps show pattern correlation, normalized root-mean-square error, and sign agreement for each combination of assumed swell period and distance factor.

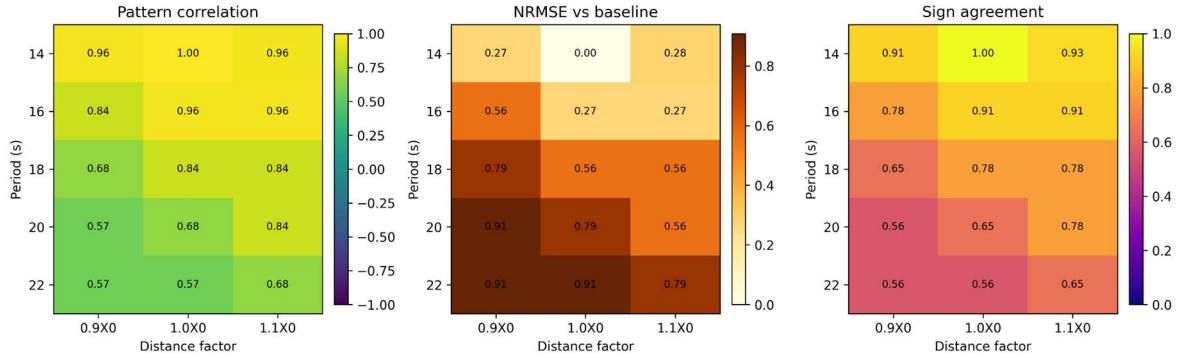

Figure S14. *Summary sensitivity metrics for the Northern Hemisphere SLP composites relative to the baseline window.* Heat maps show pattern correlation, normalized root-mean-square error, and sign agreement for each combination of assumed swell period and distance factor.

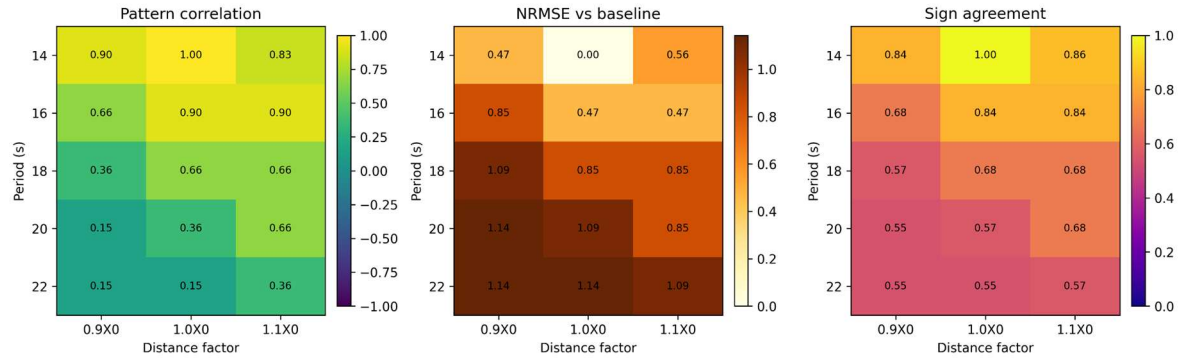

Figure S16. *Summary sensitivity metrics for the Northern Hemisphere SHWW composites relative to the baseline window.* Heat maps show pattern correlation, normalized root-mean-square error, and sign agreement for each combination of assumed swell period and distance factor.

The results show that the SH composite patterns are highly robust, while in the NH the large-scale SLP configuration remains stable across a broad range of plausible shifts, although the SHWW source pattern becomes more sensitive for the longest assumed periods. We therefore retain the original windows as reasonable first-order preconditioning windows, while clarifying that they should not be interpreted as unique exact propagation times. Event-by-event fetch coordinates, derived travel-time ranges, and full sensitivity diagnostics are now provided in the Supporting Information.

3. For NH events, wind speeds weaken in E6–E8 but strengthen in E9–E11. Although modes such as PDO, ENSO, PNA, AO, and WP are listed, their influences are inconsistent across events, and no unified physical explanation or statistical model is provided. It is recommended to divide the NH events into two groups (E6–E8 vs. E9–E11) and perform separate composite and flow-analogue analyses for each group, comparing the phase distributions of modes such as PDO and ENSO between the two groups. In addition, multiple linear regression or random forest methods should be used to quantify the relative contributions of each climate mode to the 10-m wind speed anomalies and to identify the dominant factors.

Following the recommendation, we have explored the NH events into two groups (E6–E8 and E9–E11) and performed a comprehensive statistical characterization of the climate modes associated with each group.

Composite and flow-analogue analyses: As noted in the original manuscript, flow analogues were identified individually for each event. We explored group composites for E6–E8 and E9–E11 separately; however, given that only three events constitute each group, slight spatial offsets in cyclone position among events tend to blur the composite signal, reducing its representativeness. With n=3, a single event can disproportionately influence the composite pattern. Beyond the sample size limitation, searching for analogues of a composite field raises a more fundamental methodological concern: a composite represents a statistical average that may never have actually occurred in the atmosphere, and therefore analogues of such a pattern may not correspond to physically realizable atmospheric states. This could introduce spurious results that reflect statistical artifacts rather than genuine dynamical

similarities. For these reasons, we consider that the event-by-event analogue approach, already presented in the original manuscript, provides a more physically meaningful and methodologically rigorous representation than analogue search applied to group composites.

Phase distribution of climate modes: To compare the phase distributions of PDO, ENSO, PNA, AO, WP, and IPO between the two groups, we classified each monthly index value, associated with analogues days, as negative or positive and applied chi-square tests and Mann–Whitney U tests to assess whether the distributions differ significantly between groups. The results show that PDO, ENSO, PNA, AO, and IPO differ significantly between E6–E8 and E9–E11, while WP shows no significant difference. We have included Figure S28 in the Supporting Information. Furthermore, in the Discussion Section, we highlight that the two groups of events are influenced by different phases of climate variability modes **(L507-515).** Events E6–E8 are systematically associated with positive phases of PDO, ENSO, PNA, and IPO and a negative phase of AO, whereas E9–E11 are dominated by negative phases of PDO, ENSO, PNA, and IPO.

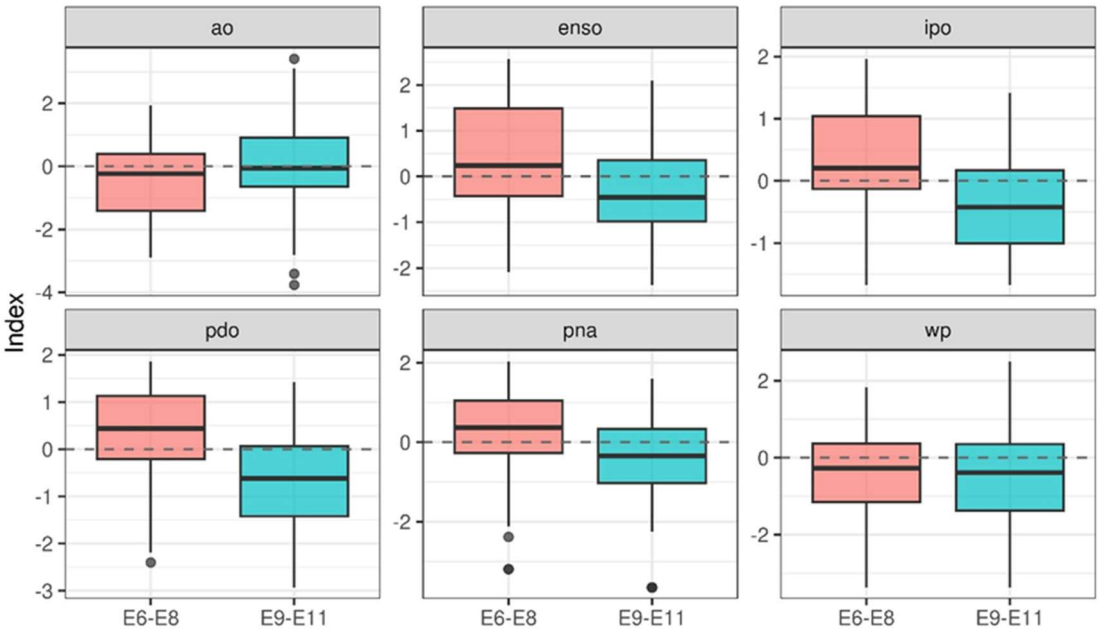

Figure S28. Boxplots showing the distribution of index values for each group across modes. Panels use independent y-axis scales, and the dashed line marks the zero reference. Di fferences are statistically significant in all groups except WP, based on chi-square tests and Mann–Whitney U tests.

Moreover, when the analysis is stratified by period, differences in the phase distributions are found to emerge primarily in the present period, where PDO, ENSO, PNA, and IPO are all statistically significant. Therefore, the E6–E8 and E9–E11 analogues do not appear to be responding to the same dynamic state of the North Pacific, suggesting that the change in wind is a response to changes in the dominant mechanisms.

Statistical models: Following the reviewer's recommendation, we applied stepwise multiple linear regression separately for each group, using monthly index values restricted to months containing analogue days, to quantify the relationship between the monthly mean wind and climate modes. For

E6–E8, the selected model retains AO and IPO as dominant predictors (adjusted $R^2 = 0.22$). For E9–E11, the model selects PNA and IPO as predictors, but the explained variance remains low (adjusted $R^2 = 0.10$), indicating that large-scale climate indices account for only a limited fraction of wind variability in this group, and that mesoscale or local synoptic factors likely play a more important role. This analysis is included in the discussion section.

E6-E8 $Wind \propto -0.20\,AO + 0.27\,IPO$

E9-E11 $Wind \propto 0.11\,PNA - 0.09\,IPO$

Although we considered using random forests as a complementary approach, we ultimately retained multiple linear regression because of its simplicity and interpretability, particularly its ability to quantify relationships through coefficients. While random forests can capture nonlinearity, their feature importance metrics identify relevant predictors without providing a clear measure of effect size or direction. A more detailed investigation of North Pacific variability, potentially using nonlinear methods, is therefore left for future work.

In summary, NH events were divided into two groups (E6–E8 and E9–E11) and analyzed separately. The event-by-event analogue approach was retained as the primary method, since composites based on only three events are insufficiently robust and searching for analogues of statistically average fields may not correspond to physically realizable atmospheric states. Statistical characterization shows clear and significant differences in the phase distributions of major climate modes between the groups, with these contrasts becoming more pronounced in the present period, suggesting a shift in the dominant dynamical mechanisms. Regression results further indicate that large-scale modes play a moderate role for E6–E8 but explain only a small fraction of variability for E9–E11. Overall, these findings support the interpretation that the observed wind changes arise from differing climate mode configurations and their evolving influence, while also pointing to the need for future work to better capture nonlinearities and regional dynamics.

4. The flow-analogue method uses only SLP, Z500, and Z250, without including boundary conditions such as sea surface temperature (SST) or sea ice. This may mistakenly classify weather patterns that are dynamically similar but thermodynamically different as the same type, thereby introducing spurious climate change signals. It is recommended to add the SST field (e.g., monthly SST anomalies) as a fourth variable in the analogue similarity calculation, or at least to perform a sensitivity test: keep the existing three variables unchanged, but use the SST anomalies corresponding to the analogue dates as a posteriori diagnostic variable to test whether SST differs significantly between the earlier and later periods.

We would like to clarify that the flow-analogue method was intentionally designed to operate exclusively on dynamical fields (SLP, Z500, and Z250), which is standard practice in the analogue literature (Jézéquel et al. 2018, Thompson et al. 2026). The rationale is to identify days with genuinely similar atmospheric circulation and then assess what thermodynamic conditions are associated with those patterns, rather than combining dynamics and thermodynamics in the similarity metric itself, which could obscure the relative contribution of each.

Following the reviewer's suggestion, we performed an additional analysis in which SST anomalies (relative to the 1991–2020 climatology) were used as a posteriori diagnostic variable. After identifying analogues based solely on circulation, we classified the SST anomalies associated with those dates into terciles (cold, neutral, warm). We then conducted two complementary approaches: (i) classifying analogues solely according to SST anomaly category, irrespective of period; and (ii) quantifying, for each period, the fraction of analogues associated with each SST class.

For events originating in the SH, the first analysis revealed that days with warm SST anomalies both for random circulation and for analogue situations, are associated with stronger 10-m winds (Figure S22). This is physically consistent with enhanced lower-tropospheric instability and increased surface energy fluxes under warm SST conditions, which intensify convective activity and near-surface winds independently of the large-scale circulation pattern (Chen, 2025). The only exception is event E3, which shows an opposite SST–wind relationship; this event is also the only one not influenced by SAM, suggesting that different dynamical controls may be at play.

In the NH, by contrast, warm SST anomalies under random atmospheric circulation are associated with weaker surface winds (Figure S23). This opposing sign relative to the SH is consistent with the cross-correlation analysis of Chen (2025), who showed that at lag 0 most NH ocean regions exhibit a negative SST–wind correlation, in contrast to the predominantly positive relationship found in the SH. This hemispheric asymmetry likely reflects the greater role of baroclinic damping in the extratropical NH, where warmer sea surfaces reduce the meridional temperature gradient and weaken the baroclinic forcing that drives extratropical wind systems. When the circulation is constrained to analogue patterns, however, this signal is not uniform: E6 and E8 maintain the same weakening behavior observed on random days, whereas E7 and E9–E11 show wind intensification under warm SSTs, suggesting that the large-scale dynamical context associated with each event's circulation pattern can modulate or even reverse the background thermodynamic response.

The second analysis revealed that, in the current period, a greater proportion of analogues occur under anomalously warm SST conditions for all events, consistent with the background warming trend associated with climate change (Figures S24-S25). Therefore, there is strong agreement between the period-based and SST-based analyses across most events. In the SH, the observed increase in wind intensity in the present period corresponds to a higher frequency of warm SST analogues (Figure S24). The exception is E3, where the period-based analysis suggests an increase in wind intensity, while warm SST conditions in the SST-based analysis are associated with a decrease.

For NH events, the two analyses are also broadly consistent. E6 and E8 show wind weakening under warm SSTs, in agreement with the period-based results. E9–E11 show wind intensification under warm SSTs with analogous circulation, also consistent with their period-based signals. The main exception is E7, for which the dominant influence of the AO may be overriding the SST-driven response, decoupling the thermodynamic and period-based signals.

In summary, the high degree of consistency between the period-based and SST-based analyses strengthens confidence in the robustness of our results. For clarity, we have retained the period-based analysis in the main text, added discussion of the SST-based results and their physical interpretation in the Discussion section **(L461-465)**, and included the corresponding figures as supplementary material.

With regard to sea ice, we did not find a strong correlation between 10-meter wind speed and sea ice extent in the North Pacific. Likewise, at the request of the other reviewer, for the SH we analyzed changes in 10-meter wind before and after 2016, the year from which Antarctic sea ice extent decreased considerably, but we did not find a significantly relevant signal either.

Chen, W. (2025). Gradual strengthening of global oceanic surface winds: Correlations with sea surface temperature and implications for wind power extraction. Heliyon, 11. https://doi.org/10.1016/j.heliyon.2025.e42788.

Jézéquel, A., Yiou, P. & Radanovics, S. Role of circulation in European heatwaves using flow analogues. Clim Dyn 50, 1145–1159 (2018). https://doi.org/10.1007/s00382-017-3667-0

Thompson, V., Philip, S., Kew, S., Pinto, I., & Vautard, R. (2026). Using analogue methods to identify trends in circulation patterns of midlatitude heatwaves. Weather and Climate Extremes, 52, 100898. https://doi.org/10.1016/j.wace.2026.100898

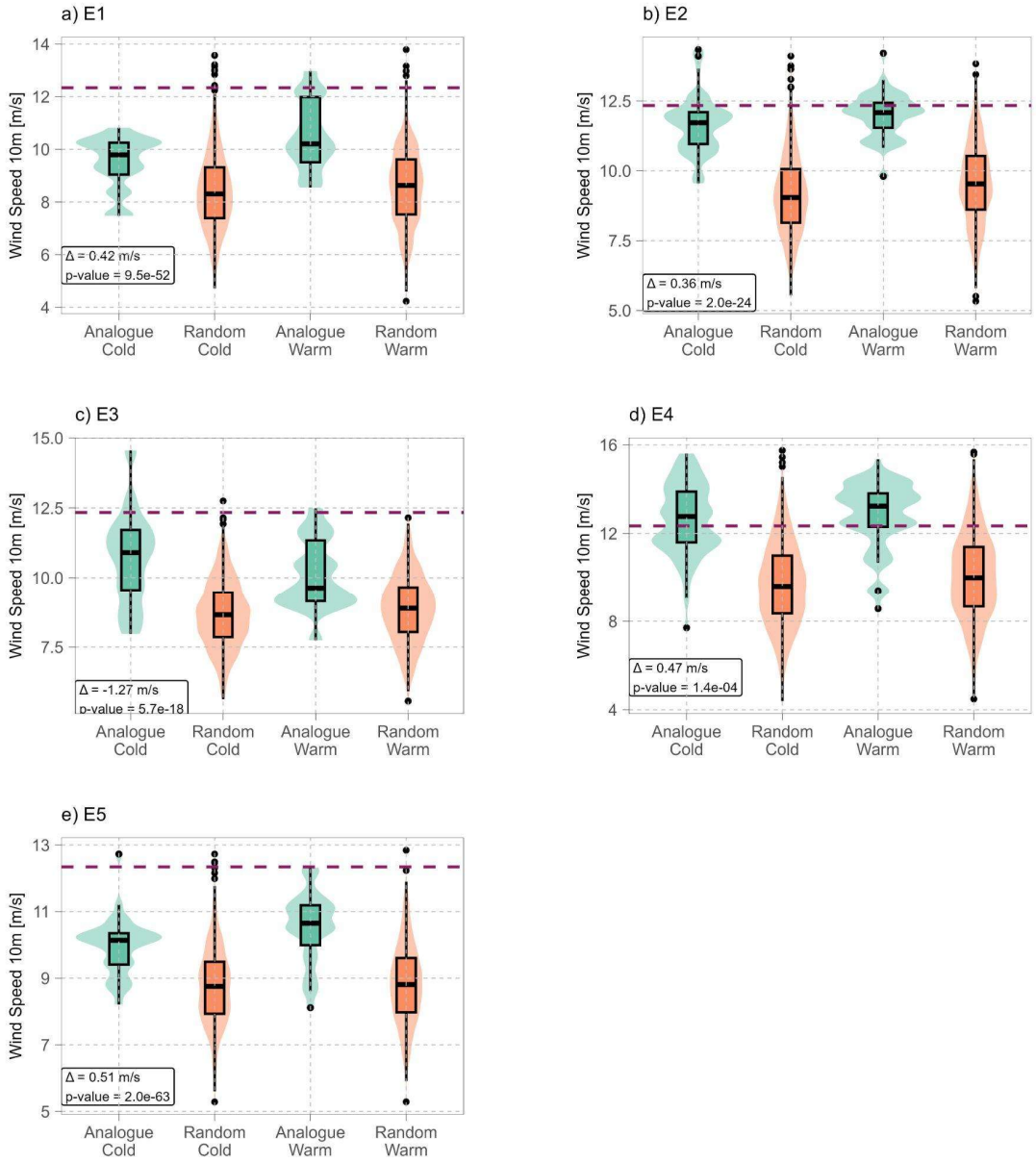

Figure S22. *Violin and box plots of 10-m wind speed associated with analogue days for events originated in the Southern Hemisphere, conditioned on SST anomaly terciles.* Distributions are shown separately for analogue and random-circulation days under cold and warm SST anomalies, as indicated on the x-axis. The dashed horizontal line marks the observed 10-m wind speed. The label reports the difference in median wind speed between warm and cold analogue days and the p-value from a Mann–Whitney U test assessing whether the two samples differ significantly.

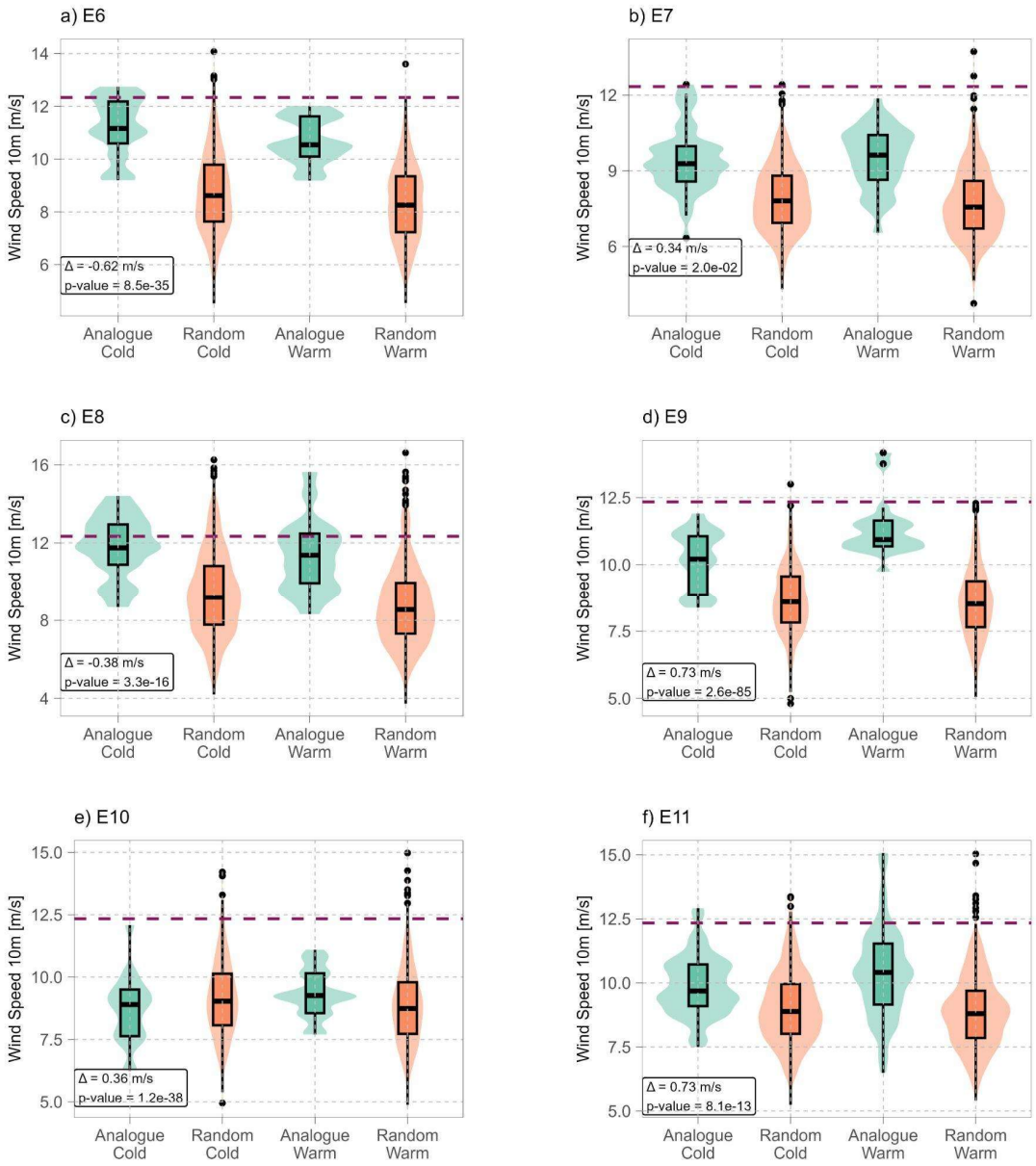

Figure S23. *Same as Figure S22, but for events originating in the Northern Hemisphere.*

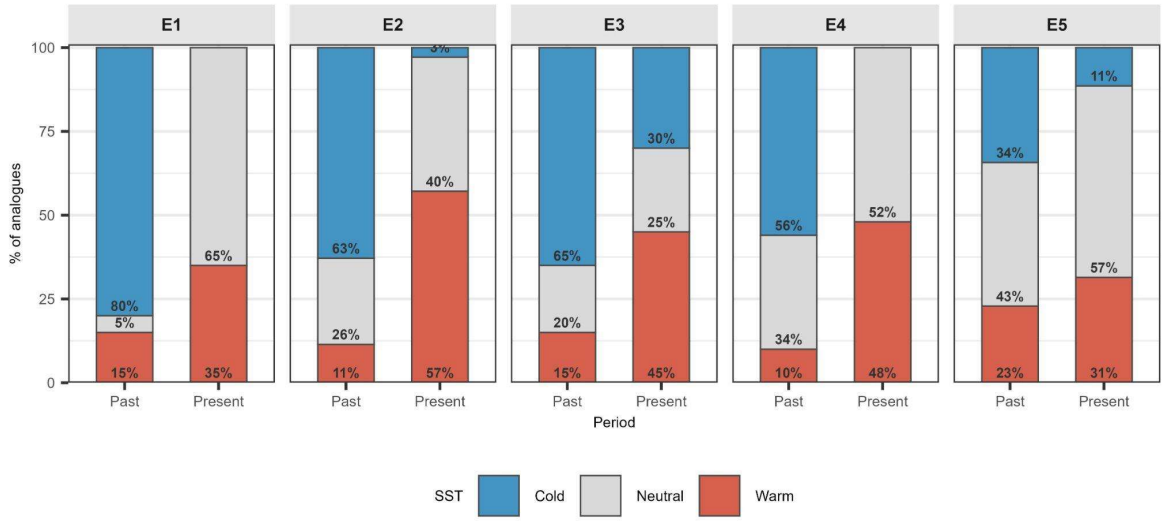

Figure S24. *Relative frequency of analogue days for Southern Hemisphere events occurring under cold, neutral, and warm SST anomalies in the past and present periods.*

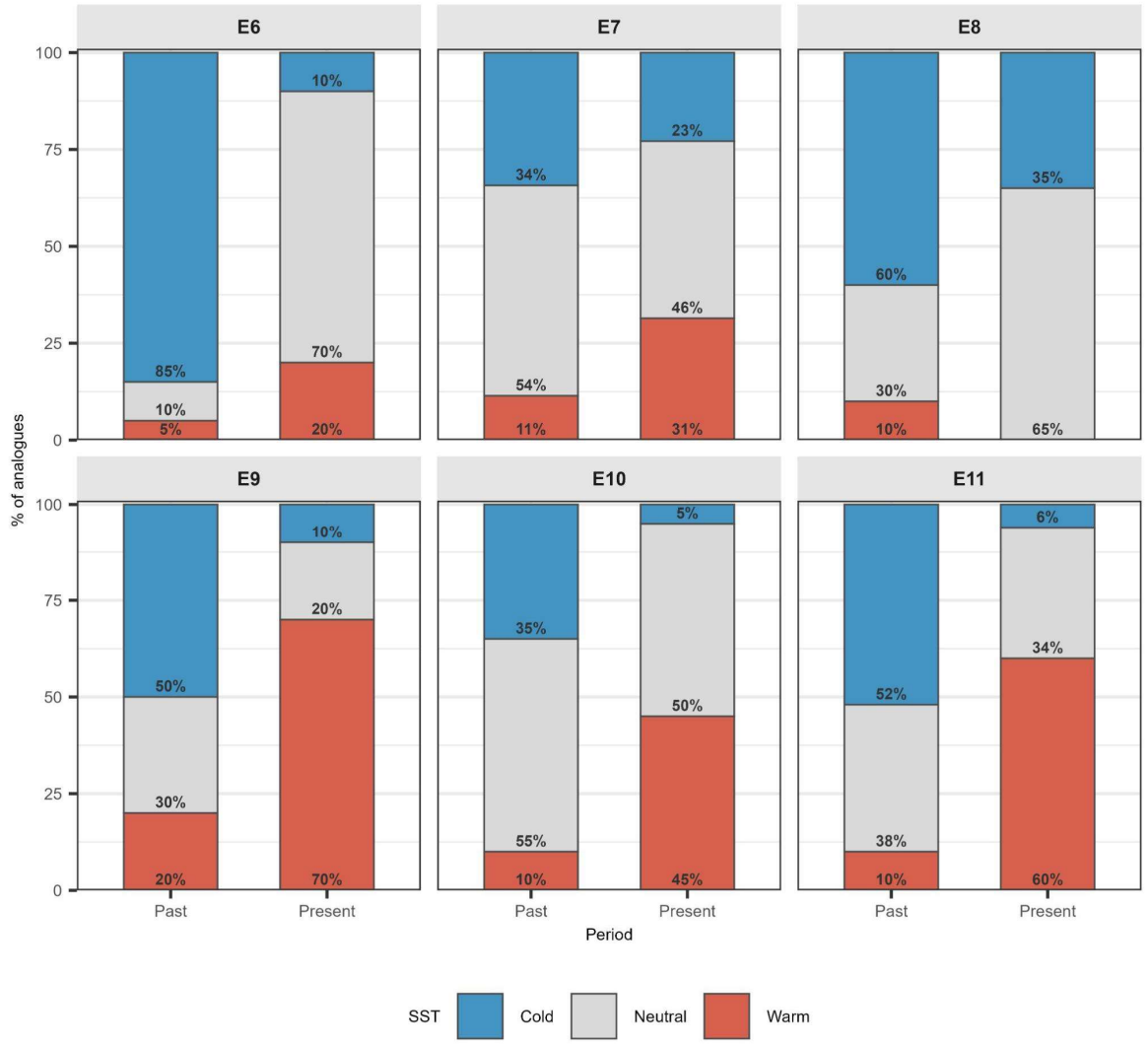

Figure S25. *Same as Figure S24, but for events originating in the Northern Hemisphere.*

5. The study uses only the significant height of wind waves (SHWW) in the generation region as an indicator of swell generation, without providing measured wave height, period, or energy spectral data at the Peruvian coast. The causal chain between the source region and coastal impacts is therefore incomplete. It is recommended to use measured wave data from at least one coastal site in Peru (e.g., Callao, Miraflores, or Paita), which may come from wave buoys, tide gauge inversion, or ERA5 nearshore points, and to produce time-series plots for one or two typical events (e.g., E1 and E9) showing the evolution from SHWW anomalies in the source region to nearshore wave heights, thereby directly illustrating the wave evolution during propagation. If measured data are unavailable, significant wave height time series should be extracted from ERA5 nearshore points (within 50 km of the coast) and subjected to lagged correlation analysis with the SHWW anomalies in the generation region (with the lag time set to the estimated travel time) to quantitatively verify the causal relationship.

We agree that the source-to-coast linkage should be documented more explicitly. In the revised manuscript, we will complement the source-region SHWW analysis with ERA5 nearshore diagnostics at representative coastal points off Peru.

Because homogeneous in situ directional wave records are not available for all selected events, we extracted nearshore time series of total swell height (SHTS) and wave-power-related diagnostics for representative events and compared them with source-region SHWW anomalies. Using the theory-based propagation windows adopted in the manuscript (3–4 days for SH events and 8–11 days for NH events), we performed lagged-correlation diagnostics between source-region SHWW anomalies and coastal SHTS anomalies, and we added event-centred time-series figures to the Supplement **(Figs. S20-S21)**.

These additional diagnostics provide physically consistent support for the source-to-coast linkage **(L452-456)**. In the Southern Hemisphere cases, the primary lags are close to the expected travel times and the coastal response is comparatively clear. In the Northern Hemisphere, the response is weaker and more dispersed, which is consistent with the longer trans-equatorial propagation path. We therefore use this analysis as complementary evidence supporting the physical consistency of the selected lead windows, rather than as a strict deterministic estimate of exact coastal arrival time for every event.

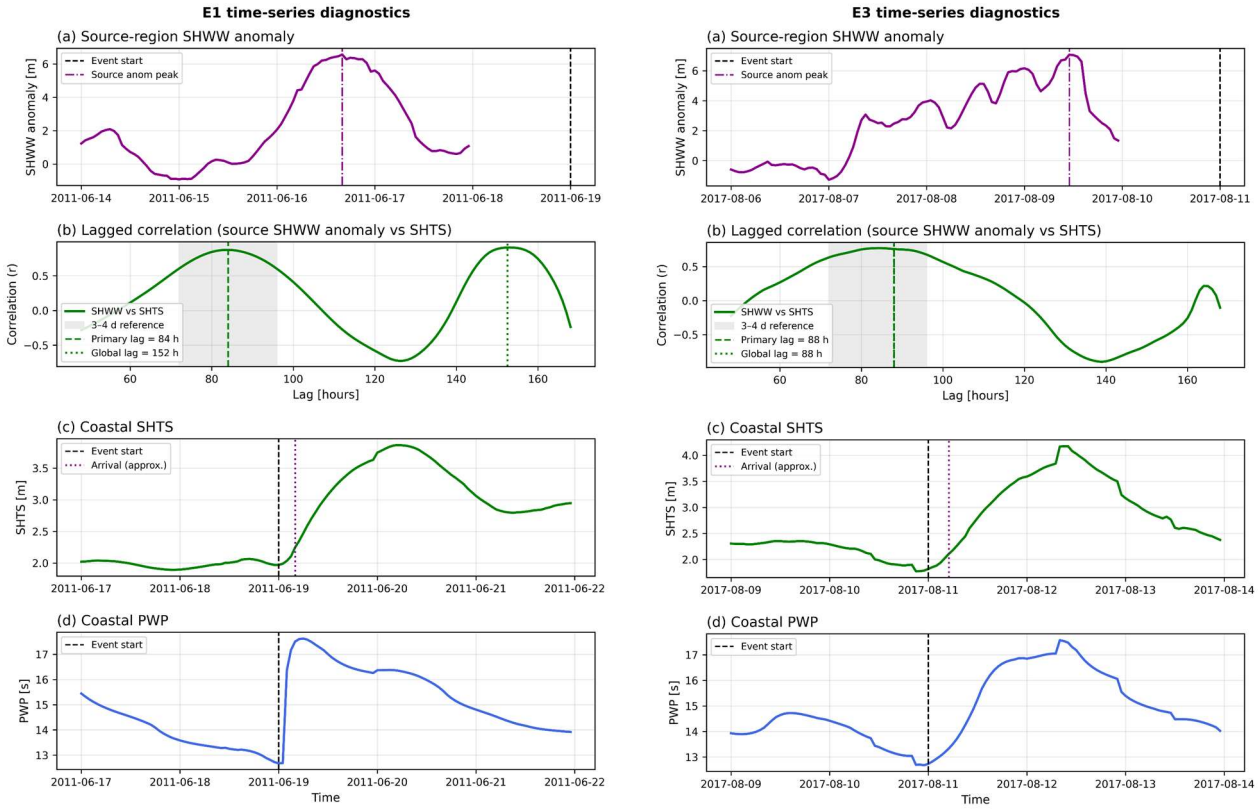

Figure S20. *Time-series diagnostics for the representative Southern Hemisphere events E1 (left) and E3 (right).* For each event, panels show (a) the source-region SHWW (Significant Height of Wind Waves) anomaly, (b) the lagged correlation between source-region SHWW anomaly and coastal SHTS (Significant Height of Total Swell), (c) the coastal SHTS time series, and (d) the coastal PWP (Peak Wave Period) time series.

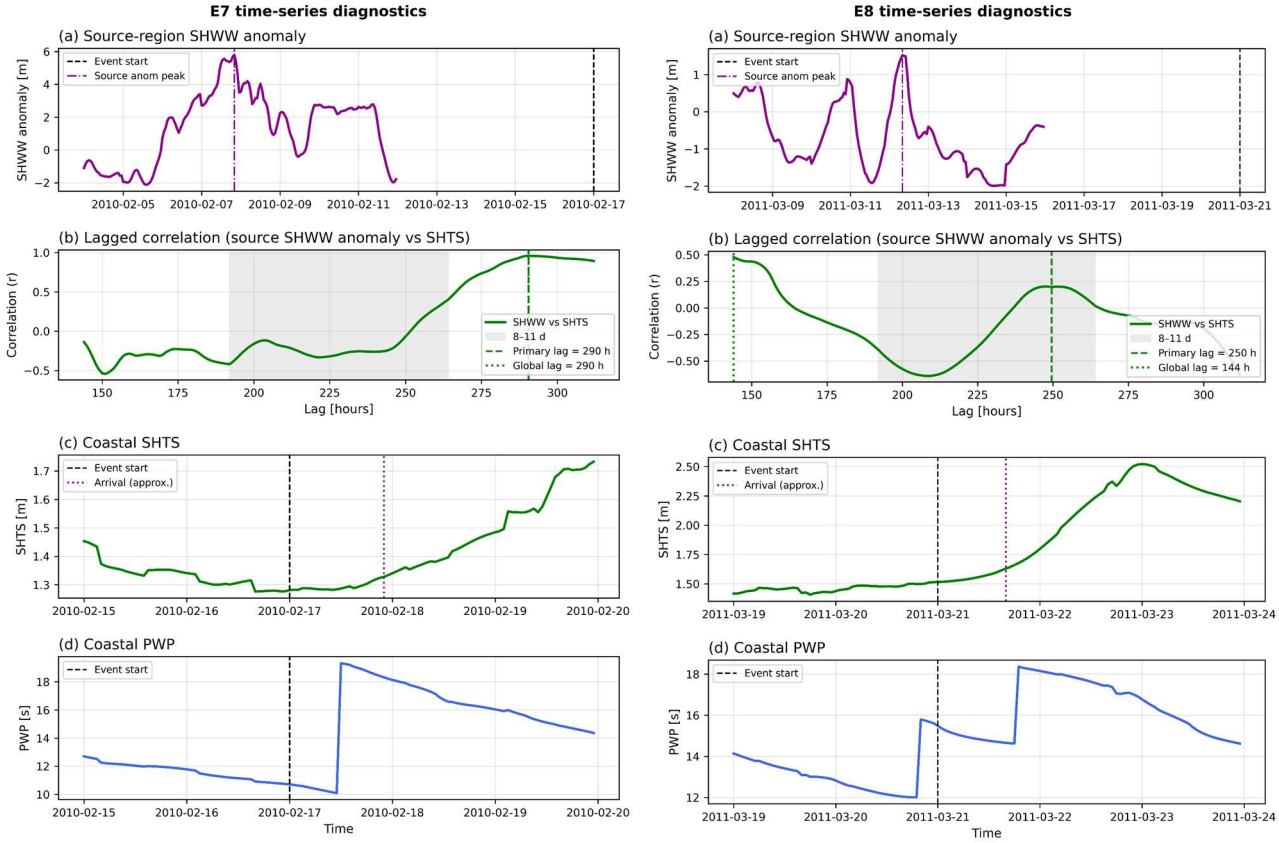

Figure S21. *Time-series diagnostics for the representative Northern Hemisphere events E7 (left) and E8 (right).* For each event, panels show (a) the source-region SHWW (Significant Height of Wind Waves) anomaly, (b) the lagged correlation between source-region SHWW anomaly and coastal SHTS (Significant Height of Total Swell), (c) the coastal SHTS time series, and (d) the coastal PWP (Peak Wave Period) time series.